

A numerical exercise for turbulent natural convection and pollutant diffusion in a two-dimensional partially partitioned cavity

Patrice Joubert ^{a,*}, Patrick Le Quéré ^b, Claudine Béghein ^a, Bernard Collignan ^c,
Stéphane Couturier ^c, Stéphane Glockner ^d, Dominique Groleau ^e, Pierre Lubin ^d,
Marjorie Musy ^e, Anne Sergent ^a, Stéphane Vincent ^d

^a LEPTAB, Université de La Rochelle, Av. M. Crépeau, 17042 La Rochelle cedex 1, France

^b LIMSIS – CNRS, BP 133, 91403 Orsay cedex, France

^c CSTB, 84 Av. Jean-Jaurès, 77421 Marne La Vallée cedex 02, France

^d MASTER – ENSCPB, 16 Av. Pey-Berland, 33607 Pessac cedex, France

^e CERMA – CNRS rue Massenet, BP 81931, 44319 Nantes cedex, France

Received 7 May 2004; received in revised form 13 August 2004; accepted 20 September 2004

Abstract

We present the results of a numerical exercise aimed at comparing the predictions of different conventional turbulent modelling approaches for natural convection at Rayleigh numbers characteristic of applications such as energy savings, fire safety or thermal comfort. A two-dimensional configuration was considered that consists of two adjacent rooms separated by a lintel in which natural convection is induced through heating on their opposite sides and subjected to diffusion of a pollutant from one room to the other. Seven contributions are available. The comparison is carried out, in terms of local or global quantities, for the mean thermal and dynamic fields and for the unsteady diffusion of the pollutant from one room to the other. Characteristic differences between steady RANS and unsteady two-dimensional DNS and LES approaches are observed and discussed.

© 2005 Elsevier SAS. All rights reserved.

Keywords: Natural turbulent convection; Building type configuration; Numerical comparison exercise; Pollutant diffusion; Turbulence models; DNS, LES and RANS approaches

1. Introduction

Because airflow in rooms are generally driven by buoyant forces, unless mechanical heating or cooling systems are present, it is important to get an accurate insight into natural convection indoor airflow, in transitional or turbulent regimes as it is almost invariably the case for real life situations. This is of major importance when considering as an example situations such as fires. So, the understanding and the numerical prediction of natural convection in building type configurations has been, and continue to be, an impor-

tant field of research for fire studies, [1–5], as well as for accidental pollutant dispersion in buildings [6]. Likewise, indoor air quality studies are also increasingly concerned with CFD in order to get a detailed description of the dynamic, thermal or indoor pollutant fields, to evaluate local comfort indicators, ventilation systems efficiency [7], or to derive simplified models [8].

Careful validation of CFD approaches for such complex problems is however hardly reachable with experiments, because complete similitude cannot be preserved with reduced scale models, and because full scale experiments need substantial financial and human resources. Moreover, the idealised boundary conditions considered in CFD computations are generally different from the real ones. One way to get insight into the pertinence of the numerical results is then to

* Corresponding author. Tel.: +33 (0)5 46 45 72 65, fax: +33 (0)5 46 45 82 41.

E-mail address: patrice.joubert@univ-lr.fr (P. Joubert).

Nomenclature

c_p	specific heat capacity	$\text{J}\cdot\text{kg}^{-1}\cdot\text{K}^{-1}$
D	mass diffusivity	$\text{m}^2\cdot\text{s}^{-1}$
g	gravitational acceleration	$\text{m}\cdot\text{s}^{-2}$
H	height of the cavity	m
Le	Lewis number	
m	mass	kg
\dot{m}	mass flow rate	$\text{kg}\cdot\text{s}^{-1}$
Nu	local Nusselt number	
\overline{Nu}	overall Nusselt number at the walls	
p	pressure term	
Ra	Rayleigh number	
t	time	s
T	temperature	K
ΔT	temperature difference between hot and cold walls	K
U	horizontal velocity	$\text{m}\cdot\text{s}^{-1}$
V	vertical velocity	$\text{m}\cdot\text{s}^{-1}$
x	horizontal coordinate	m
z	vertical coordinate	m

Greek letters

α	thermal diffusivity	$\text{m}^2\cdot\text{s}^{-1}$
ν	kinematic viscosity	$\text{m}^2\cdot\text{s}^{-1}$
ρ	density	$\text{kg}\cdot\text{m}^{-3}$
θ	non-dimensional temperature	

Subscripts

air	relative to air
BL	relative to the vertical boundary layer
cold	relative to the cold wall
hot	relative to the hot wall
lintel	under the lintel
mean	mean quantity
SF6	relative to SF6

Superscripts

+	positive velocity value or quantity entered the right cavity
*	non-dimensional quantity
tot	total quantity in the cavity

compare different turbulence models or different numerical procedures for well defined problems. One can then expect to have an idea of the pertinence of the numerical tools for complex real configurations. In this way, we proposed in 2000, during an informal French–American workshop, a numerical comparison exercise. Our main idea was to propose a comparison exercise for realistic situations in terms of dimensions and flow regimes, using either laboratory numerical tools as well as CFD engineering softwares as often done for indoor air studies.

In fact, we focused our effort on a simple 2D exercise, considering natural convection in the range of ordinary temperature differences for rooms, that is under the Boussinesq assumption. The configuration much resembles a side-heated cavity problem, with a sudden pollutant release in order to evaluate the influence of different turbulence models on the dispersion of the pollutant from one room to a second, separated of the first one by a lintel. The thermal Rayleigh number is set to 2.5×10^{10} , which is approximately two orders of magnitude above the onset of unsteadiness for such a configuration. Seven contributions are available at the moment, covering RANS $k-\epsilon$, LES and DNS approaches, with either commercial softwares or in-house made codes. The aim of this paper is to present the first results of this numerical comparison exercise.

If this exercise can appear at a first glance simple and meaningless with respect to the complexity of engineering problems, we must keep in mind how difficult is the numerical prediction of turbulent natural convection flows, for 2D enclosures, and so a fortiori for 3D configurations. A first attempt to define a reference solution for turbulent natural

convection in a 2D rectangular Differentially Heated Cavity (DHC) was done by Henkes and Hoogendoorn [9], on the occasion of the EURO THERM/ERCOFTAC conference held in Delft in 1992. However, the conclusions pointed out the fact that RANS solutions greatly differed between themselves, but also from DNS solution. Later on, an average solution was defined from the RANS contributions as the “reference solution” [10].

On the other hand, the beginning of the turbulent regime has been investigated for 2D cavities quite a long time ago, and accurate solutions exist, with in particular the spectral DNS of Xin and Le Quéré [11], for square or rectangular cavities at Rayleigh numbers of 10^9 and 10^{10} .

Considering now 3D configurations, Tric et al. [12], produced accurate solutions for the DHC, but in the range of laminar flow domain only. Instability mechanisms of 2D flows with respect to 3D periodic perturbations were investigated by Henkes and Le Quéré [13], but they still are a challenging field of research for three-dimensional effects and for the turbulent domain, and it still remains to fully characterise the 3D structure of the flows.

More recently, Zhang and Chen [14], and Peng and Davidson [15], published 3D LES results for the DHC at a Rayleigh number of 5×10^{10} which appear to be in good agreement with experimental data although only few details are reported concerning the local values. A more detailed contribution is given by Dol and Hanjalic [16]. These authors numerically investigated side-heated cavities with different thermal conditions for the horizontal walls but also for the lateral walls, in order to reproduce as well as possible the observed thermal boundary conditions of an exper-

imental facility. They performed 2D and 3D computations with two RANS models, a low Reynolds number $k-\varepsilon$ model and a sophisticated second moment closure model, and provided detailed comparisons between the numerical results and experimental data for the different thermal boundary conditions they considered. Two conclusions of their paper are of special interest for the present study. The first one is that for most of the cases they considered, the results were very close between 2D results and 3D mid-plane results, especially for the first order moments. The second is that, surprisingly, the $k-\varepsilon$ model with a simple gradient-diffusion hypothesis and low-Reynolds number modifications exhibits a pretty good agreement with the second order closure model almost everywhere, except near the corners of the cavity. If the second order closure model gives a better flow description, some discrepancies are nonetheless present between the numerical results and the experimental data, especially in the horizontal boundary layers.

Lastly, we must notice that at this time, none of the above mentioned LES or RANS results have been compared to 3D DNS results, which is the ultimate reference approach for numerical simulations, having in mind that this is the only way to compare numerical simulations with strictly identical boundary conditions.

At this stage, one can ask the following question: what would be the interest of a comparison exercise dealing with turbulent natural convection if 3D DNS results are not available for this exercise? For a long time, 2D DNS has been suspected not to be a valid approach for the DHC, as the 3D intrinsic nature of the turbulence cannot be captured by 2D DNS and because discrepancies between the results and experimental data still remain unexplained [17]. As a matter of fact, several recent papers [18,19], prove that the differences between 2D and 3D DNS for Rayleigh of order 10^8-10^9 are not important for the first order statistical moments, except in the vicinity of the corners. Consequently, the persistent differences with experimental data cannot be attributed to the 2D assumption, as 3D simulations also fail to exactly reproduce the observed results. This means that these differences originate from uncontrolled experimental or improperly simulated boundary conditions, or from non-simulated physical mechanisms, such as radiative transfer as an example. It means that, in the same way that was observed in [16] for RANS approaches, 2D DNS can be considered as a pertinent attempt to characterise the mid-plane flow in the absence of 3D available results. This comes from the essentially 2D geometrical nature of the DHC problem, and would not probably hold for problems with three-dimensional geometrical or boundary conditions aspects. As a way of conclusion, we will state in that study that 2D DNS can be considered as the reference approach for the present exercise.

Let us now return to the configuration considered here, that is essentially a 2D turbulent cavity partitioned by a lintel and heated from the side.

Similar problem has yet been addressed numerically by Fusegi et al. [20] for an air filled cubical enclosure with

3D aperture or 2D partition extending from the ceiling at Rayleigh numbers of respectively 10^7 and 5×10^9 . The limited computational resources at this time did not allow the authors to do a real DNS, but their 3D unstationary computations without explicit turbulence modelling were probably a pioneer work on the subject. Later on, Hanjalic et al. [21] performed 2D RANS with an Algebraic Flux Model for partitioned and no-partitioned side heated cavities at Rayleigh numbers from 10^{10} to 10^{12} , in order to compare with the experimental studies of Nansteel and Greif [22,23], and Olson et al. [24] in water or air.

The configuration we deal with here is quite similar to those described in the preceding papers, except that we also consider a pollutant diffusion scenario. A comparison is performed for the seven contributions available at the moment for this exercise in terms of local values but also in terms of integral quantities, in order to pinpoint the influence that local discrepancies can induce on global values. If characteristic differences between steady RANS and unsteady DNS and LES approaches are still observed for mean values, as well as for the thermal field than for the dynamic field, the predicted heat transfer at the walls is nevertheless in a fairly good agreement when compared to similar previous comparison exercises. The pollutant behaviour and the corresponding characteristic time for diffusion from one room to the other are also presented and discussed.

The paper is organised as follows: the description of the exercise is given in the next section, followed by a short presentation of the different contributions. Eventually, Section 4 is devoted to the presentation of the results and their comparisons before concluding remarks.

2. Description of the exercise

2.1. Description

The configuration of the exercise is shown in Fig. 1 and consists in a cavity of aspect ratio length/height of 2, composed of two adjacent square rooms separated by a lintel. The height of the cavity, H , is set equal to 3 m. The lintel has an extension of $0.3H$ from the ceiling and a width of $0.05H$. The left room is heated on its left side wall at temperature T_{hot} , and the other room is cooled at its right wall

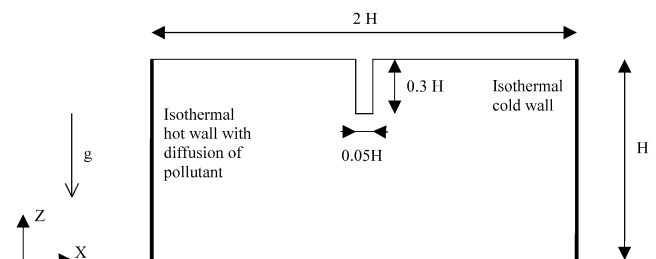


Fig. 1. Description of the cavity ($H = 3$ m).

Table 1
Participants to the benchmark

Authors	Type of code	Spatial discretization	Number of points (X, Z)	Time step (s)	Turbulence description	Position of the first inner grid point x (non-dimensional units)
Béghein	Commercial (STAR-CD)	FVM. Unstructured irregular grid	13 196 meshes 14 130 nodes	0.03	$k-\varepsilon$ RNG, two-layer	1.67×10^{-3}
Collignan and Couturier	Commercial (FLUENT)	FVM. Structured irregular grid	128×102 (12 856)	1	$k-\varepsilon$ RNG, two-layer	1.67×10^{-4}
Collignan and Couturier	Commercial (PHOENICS)	FVM. Structured irregular grid	77×54 (4 158)	2.5	$k-\varepsilon$, Chen–Kim model	1.98×10^{-3}
Glockner, Lubin and Vincent	In house made (AQUILON)	FVM. Structured irregular grid	160×80 (12 800)	0.1	$k-\varepsilon$ RNG, low Reynolds	1.125×10^{-3}
Groleau and Musy	Commercial (N3S)	FEM. Unstructured triangular elements	22 434 volumes 45 939 nodes	0.06	$k-\varepsilon$, Kato–Lauder model	–
Joubert and Sergent	In house made (LIMSI)	FVM. Structured irregular grid	128×128 (16 384)	0.01	2D LES	2.8×10^{-4}
Le Quéré	In house made	FVM. Structured irregular grid	1024×512 (524 288)	0.0047	2D DNS	4.697×10^{-6}

FVM = Finite Volumes Method;
FEM = Finite Elements Method.

at temperature T_{cold} . This gives rise to a general clockwise airflow circulation in the cavity.

Moreover, after the flow motion has been established in a statistical sense, a passive pollutant is diffused at a constant rate along the left wall during 1 minute, and its evolution with time is tracked during 10 minutes after the diffusion stops, in order to evaluate the dynamics and the characteristic time of its penetration in the right cavity.

2.2. Physical properties of air and pollutant

The air properties at the reference temperature $T_{\text{mean}} = 298$ K are respectively $\rho_{\text{air}} = 1.2$ kg·m⁻³ for density, $\nu_{\text{air}} = 1.6 \times 10^{-5}$ m²·s⁻¹ for the kinematic viscosity, $\alpha_{\text{air}} = 2.25 \times 10^{-5}$ m²·s⁻¹ for the thermal diffusivity and $c_{p\text{air}} = 1$ kJ·kg⁻¹·K⁻¹ for the specific heat. The corresponding value of the Prandtl number is $Pr = 0.71$.

The properties of the pollutant are those of SF6 (a gas widely used for comfort studies in rooms), except for the coefficient of mass expansion imposed to zero, thus considering the pollutant as a passive scalar. This choice was done in order to focus the comparison on the scalar transport, avoiding the influence of the pollutant on the flow field.

The molecular weight of SF6 is 146 g·mol⁻¹ and its mass diffusivity is $D_{\text{SF6}} = 8 \times 10^{-6}$ m²·s⁻¹. The Lewis number is in these conditions, $Le = 2.8$.

2.3. Boundary conditions

The temperature difference $\Delta T = T_{\text{hot}} - T_{\text{cold}}$ between the two opposite isothermal walls is held at $\Delta T = 10$ K around the reference temperature, leading to a Rayleigh number of $Ra = 2.5 \times 10^{10}$, that is roughly two orders of

magnitude above the onset of unsteadiness for similar configurations.

The pollutant is produced at a constant rate from the whole isothermal left wall, during 1 minute, yielding a total mass $m_{\text{SF6}}^{\text{tot}} = 10.8$ g in the cavity.

All the walls, except the isothermal ones are adiabatic. Lastly, non-slip conditions are considered for all the walls.

3. Presentation of the contributions

This exercise was originally proposed for a French–American ARIEL¹ Workshop held in April 2000 at the National Laurence Berkeley Laboratory (Berkeley, California). Nevertheless, at this time only French teams carried out the exercise, leading to seven contributions from five different laboratories.

The participants are listed in Table 1 with a brief description of each contribution (type of code, spatial discretization method, number of points or elements, time step for the diffusion of the pollutant and turbulence model). The spatial discretization of the cavity is mainly achieved within a Finite Volume Method, with structured or unstructured grids, except for Groleau and Musy who used a Finite Element Method. The numerical codes are either commercial (FLUENT, PHOENICS, STAR-CD, N3S) or in-house softwares. The turbulence description of the flow is achieved within $k-\varepsilon$ type models for five contributions, mainly with an RNG formulation, but also with LES and DNS approaches.

¹ ARIEL is the acronym for “Association for Research with Industrial and Educational links”, supported by the French Ministry of Education and Research.

The two layer option was used for the near wall treatment by Béghein, with STAR-CD, and by Collignan and Couturier with FLUENT. Walls functions were used by Collignan and Couturier with PHOENICS and by Groleau and Musy while Glockner et al. used low-Reynolds number modification near the walls.

The number of points lies from 4158 (PHOENICS' results of Collignan and Couturier) to up to more than half a million for the DNS of Le Quéré, but three RANS contributions used approximately 13 000 grid points, so they can be compared in nearly similar conditions of spatial accuracy. All the contributors refined the spatial discretization near the vertical walls, whatever the turbulence modelling, in order to capture the thin vertical boundary layers.

Finally, the equations of motions, energy and pollution diffusion were solved either in dimensional or in non-dimensional form.²

4. Presentation of the results and discussion

This comparison exercise can in fact be decomposed into two successive steps: the first objective is to obtain the mean field values for temperature, velocities and turbulent quantities, while the second part aims at observing the evolution of pollutant with time. Note that for this latter part, the approaches are quite different between RANS on the one hand and LES and DNS on the other hand. In fact, for steady RANS approaches as those considered in this exercise, the pollutant is convected and diffused by the mean velocity field and the mean turbulent Reynolds stresses, so that only the equation of conservation for the pollutant has to be integrated in time during this second period. On the other hand, LES or DNS have to deal with the complete set of equations for motion, energy and pollutant concentration at each time step during the whole process.

4.1. Mean fields before pollutant diffusion

The general structure of the flow in the cavity is described in Fig. 2 where the mean fields of temperature, stream function and turbulent kinetic energy are presented. The flow is organized in a general clockwise circulation, with a large central region approximately at rest, which is very similar to that of an undivided cavity. In the left cavity, the presence of the lintel creates a dead zone in the upper part of the cavity, where the fluid is nearly at rest and exhibits a strong thermal stratification. The fluid heated along the hot wall then separates from the wall at nearly $z^* = 0.65$, flows horizontally to the right cavity in a jet-like structure, produces a large eddy just behind the lintel and then feeds the downwards cold boundary layer along the right wall. Moreover, we can

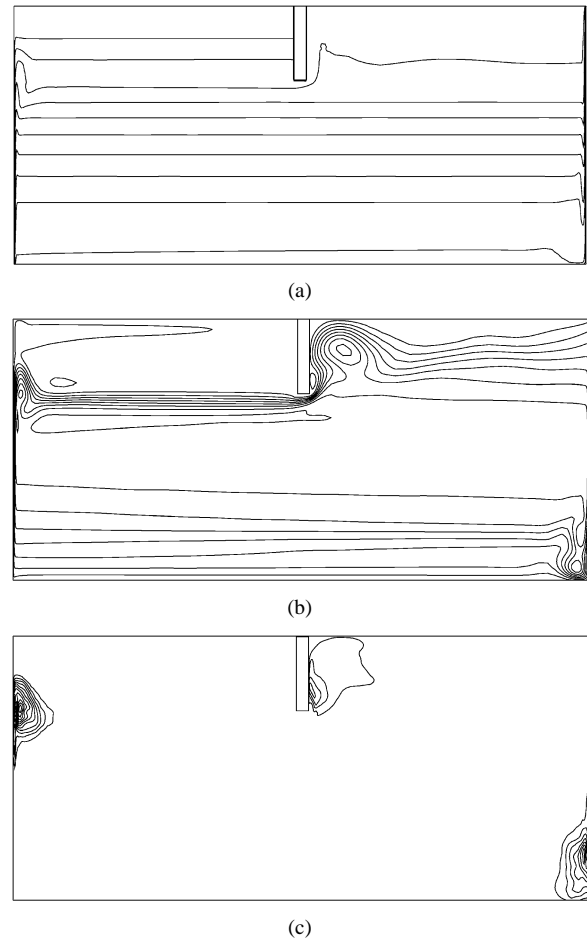


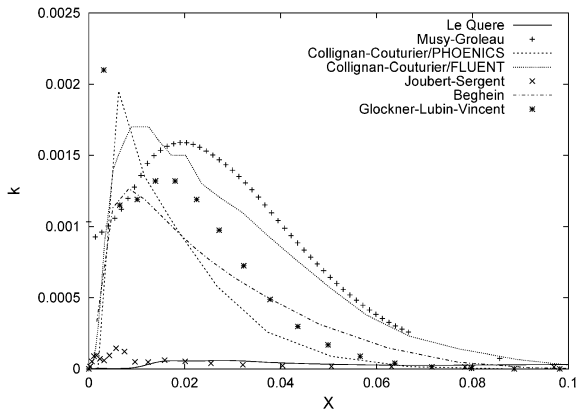
Fig. 2. (a) Example of mean temperature field. (b) Example of mean stream-function field. (c) Mean field of turbulent kinetic energy observed with LES.

observe a detachment region from the ceiling in the backward part of the eddy, as well as in the downward part of the cold boundary layer, which indicates the region where the boundary layer becomes unstable and where eddies detach from it.

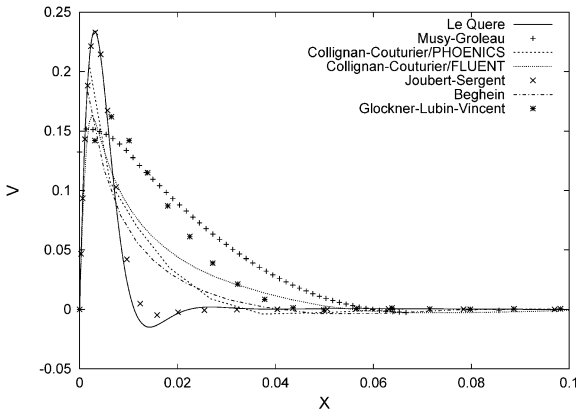
This flow structure is consistent with the previous observations of Fusegi et al. [20], but contrasts with those observed by Hanjalic et al. [21], for cavities of aspect ratio length/height of 2, who observed a shearing transverse motion at mid height of the unobstructed part of the cavity when a ceiling partition was present, or at mid height of empty cavity. In the present comparison, if some differences are present between the different contributions (which are not extensively presented here for space limitations) the above described general flow structure, without any shearing transverse flow in the central part, is nevertheless observed by all the participants.

The main discrepancy between participants is observed for the location of the turbulent kinetic energy, k . Fig. 2(c) shows the result with the LES model (Joubert and Sergent), where the kinetic energy is located in the downstream regions of the boundary layers where the eddies detach from the wall. This clearly indicates that the boundary layers re-

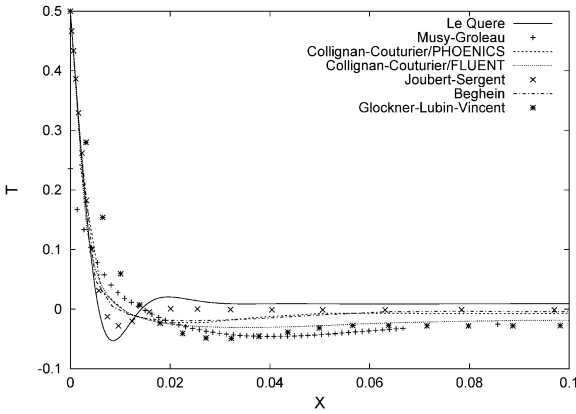
² Details of the numerics and results of the contributions are available in the online version of the paper at <http://www.sciencedirect.com>.



(a)



(b)



(c)

Fig. 3. (a) Mean kinetic energy profile at mid-height of the cavity. (b) Mean vertical velocity profile at mid-height of the cavity. (c) Mean temperature profile at mid-height of the cavity.

main laminar over a large part of the walls. This is also the case for the DNS of Le Quéré. On the other hand, all the RANS contributions exhibit much larger regions of significant k , extending in particular up to the upstream corners of the boundary layers. This is clearly visible in Fig. 3(a) where the horizontal profiles of the turbulent kinetic energy at mid-height of the cavity are reported. The different RANS contributions exhibit large values of k in the boundary layers, while LES and DNS values are nearly zero at this level.

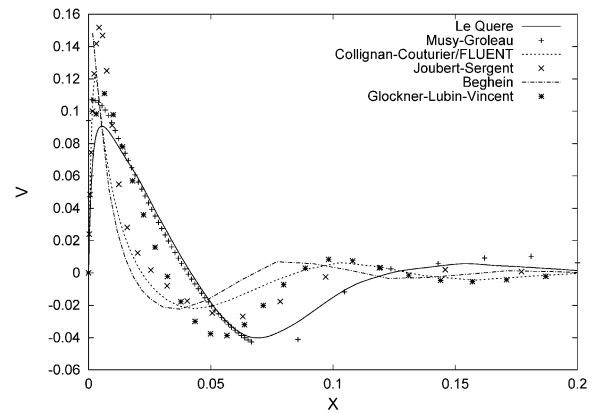


Fig. 4. Mean vertical velocity profile at $Z = 0.7$.

This structural difference results in very different profiles for the vertical velocity at the wall. An example is given at mid-height of the hot wall in Fig. 3(b). The high level of k produces a typical turbulent smooth diffusive shape for the $k-\epsilon$ approaches, while the boundary layers predicted by DNS or LES display a typical laminar nature with much smaller thickness and a higher peak of velocity compared to the RANS results. On the other hand, the differences are not so strong for the horizontal profiles of temperature (Fig. 3(c)), where the temperature gradients at the wall are in reasonable agreement. This will be confirmed later when comparing the Nusselt numbers at the walls.

The vertical velocity profiles of Fig. 4 are observed at $z^* = 0.7$, that is in the region where large eddies detach from the wall. This gives rise to a complex flow structure with recirculating fluid in the outer region of the boundary layer. A large scattering is observed between the results, for the thickness of the different regions and for the velocity peak value, indicating the difficulty in predicting the flow in this region.

Let us now focus on the flow under the lintel. As our interest is the transport of pollutant from one room to the other, it is of utmost interest to look at the flow structure at the rooms interface which is determinant in this transport. The temperature and horizontal velocity profiles under the lintel are presented in Fig. 5(a) and (b).

The flow is organised in 3 different regions, first a jet-like structure just under the lintel, then a large but very weak flow region mainly from the right to the left cavity, and finally a horizontal boundary layer near the bottom of the cavity. This is observed by all contributors, the main differences lying in the prediction of the peak velocities in the boundary layers, and as a consequence, in the intensity of the velocity in the returning core region.

Comparisons of the vertical temperature profiles gives rather different conclusions, as these profiles display several differences:

- First, if all participants, except one, achieve a fairly good agreement in predicting the attachment temperature at the sub-face of the lintel, this is not the case at the bot-

tom of the cavity, where the predicted temperatures lie between -0.28 and -0.38 .

- Second, when looking at the thermal stratification near the neutral point, we can observe a large difference between two groups of results. The first group concerns all the RANS approaches with very homogeneous results, the other one being DNS and LES, with a much higher stratification. This is also the case at the centre of each cavity (not presented), and is a noteworthy characteristic difference already observed in a previous benchmark for the case of a single 2D cavity between RANS and DNS results [9,10].

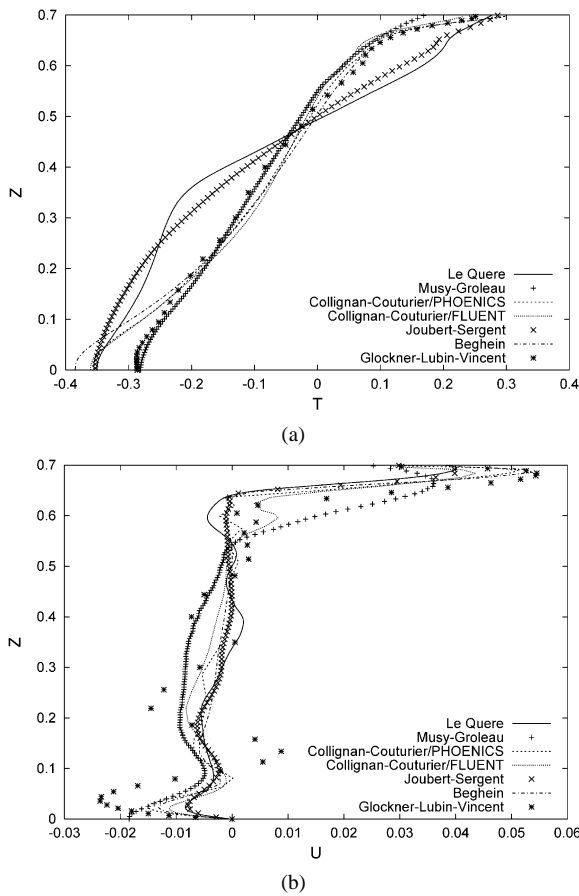


Fig. 5. (a) Mean temperature profile under the lintel. (b) Mean horizontal velocity profile under the lintel.

4.2. Heat transfer at the walls and mass flow rates in the boundary layers

As pointwise comparisons of profiles are not always very significant, especially when the differences are large, all contributors were asked to compute some global thermal and dynamic values. The chosen thermal quantities are the overall heat transfer at the hot and cold walls, respectively \overline{Nu}_{hot} and \overline{Nu}_{cold} , where

$$\overline{Nu} = \int_0^1 Nu(z^*) dz^* \quad (1)$$

and

$$Nu(z^*) = \frac{\partial \theta(x^* = 0)}{\partial x^*} \quad (2)$$

in dimensionless form. The dynamic quantities are the mass flow rate across the vertical boundary layer at the mid height:

$$\dot{m}_{BL} = \int_0^\delta \rho V(x, z = 1.5 \text{ m}) dx \quad (3)$$

and the mass flow rate under the lintel entering the right cavity:

$$\dot{m}_{lintel}^+ = \int_0^{0.7H} \rho U^+(x = 3 \text{ m}, z) dz \quad (4)$$

where V is the vertical velocity, U^+ stands for the positive value of the horizontal velocity and δ is the dynamic boundary layer thickness. All these quantities are listed in Table 2.

Generally speaking, it is observed that for each contribution, the heat transfer at the hot and cold walls are very close, indicating a good convergence of the mean fields. The corresponding Nusselt numbers along the hot and cold walls are presented in Fig. 6(a) and (b). The effect of the lintel is to create a hot stagnant fluid region in the upper part of the left cavity. The consequence is that the heat transfer is reduced in this part of the hot boundary layer (cf. Fig. 6(a) for $0.75 < z^* < 1$) when compared to the corresponding region of the cold wall ($0 < z^* < 0.25$) for which the Nusselt profile is similar to that found in a single cavity. This decrease in the heat transfer is consistent with the experimental observations of Nansteel and Greif [22,23].

Table 2
Overall Nusselt numbers and mass flow rates

Authors	\overline{Nu}_{cold}	\overline{Nu}_{hot}	\dot{m}_{lintel}^+ [g·s ⁻¹]	\dot{m}_{BL} [g·s ⁻¹]
Béghein	125.7	125.1	7.54	7.45
Collignan and Couturier/PHOENICS	136.5	135.1	9.01	8.82
Collignan and Couturier/FLUENT	113.6	115.2	9.99	9.98
Glockner, Lubin and Vincent	148.7	140.5	14.95	12.87
Groleau and Musy	122.3	115.5	16.39	21.3
Joubert and Sergent	131.3	130.8	6.80	6.32
Le Quééré	118	118	7.4	5.6

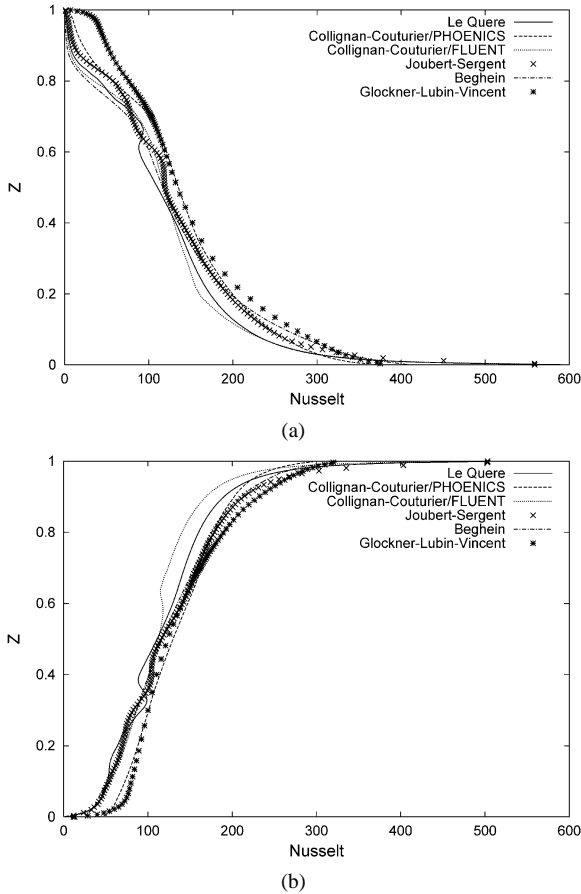


Fig. 6. (a) Mean Nusselt number along the hot wall. (b) Mean Nusselt number along the cold wall.

The results lie within a 25% range around the mean observed value of 128. Moreover, the observed values for RANS contributions either over predict or under predict the DNS results.

Two observations must be highlighted, as they contrast with the conclusions of previous comparison exercises for natural convection flows in cavities. For instance, the 92' EURO THERM/ERCOFTAC benchmark for a square buoyancy driven cavity at $Ra = 5 \times 10^{10}$ [9,10], resulted in a reference Nusselt value of 256 for the $k-\varepsilon$ approaches, with minimum and maximum values of respectively 248 and 348, while Le Quéré obtained a value of 100 with a 2D spectral DNS for a slightly lower Rayleigh number of 10^{10} .

The aforementioned predicted DNS value of 118 for a Rayleigh number of 2.5×10^{10} is then in good accordance with this previous result and follow the classical laminar $Ra^{1/4}$ scaling law for the Nusselt number, if we take account of the fact that the influence of the partition is to decrease the heat transfer at the walls. But, if the DNS values are consistent between these two exercises over a 10 years period, the current observed profiles and mean values for the Nusselt number seem to indicate a real change in the RANS prediction of the thermal heat transfer.

Considering the Nusselt repartition along the vertical walls obtained for the 92' EURO THERM/ERCOFTAC

benchmark, all profiles present a sudden increase of the Nusselt number at a vertical position varying from one author to the other and even for the same author with the grid points number, but located in the first upstream part of the vertical boundary layer. This increase was ascribed to the laminar to turbulent transition of the boundary layer, and some authors triggered the boundary layer in order to get independence of this transition point with the number of grid points they used. Later on, Hanjalic et al. observed basically the same evolution for the aspect ratio $H/L = 2:1$ cavity using an algebraic heat flux model [21].

Although the RANS contributions used here basically make use of the same classical one-point closure turbulence models than those used for the EURO THERM/ERCOFTAC benchmark, we indeed observe that the Nusselt profiles in Fig. 6(a) and (b) do not present any abrupt change in the upstream part of the boundary layer, but a smooth continuous evolution, accordingly to the DNS result. A slight discontinuity can however be observed for the PHOENICS' results of Collignon and Couturier for the cold and hot Nusselt profiles at respectively $z = 0.2$ and $z = 0.65$.

This improvement in RANS prediction of the thermal transfer at the walls can thus be probably explained by better wall treatment for natural convection in the CFD industrial softwares.

Contrarily to the reasonable agreement observed for the heat transfer at the walls, the same level of agreement is not found for the dynamic global values, and confirms the observed differences for the velocity and kinetic energy profiles in Fig. 3(a), (b). The discrepancy in the observed values is quite large between the authors, either for the flow mass through the vertical boundary layer (\dot{m}_{BL}) or for the flow entering the right cavity ($\dot{m}_{\text{lintel}}^+$).

However, we can note that there is a more or less pronounced trend for predicting a gap between \dot{m}_{BL} and $\dot{m}_{\text{lintel}}^+$. Except for Collignon and Couturier, who predict the same values when using FLUENT, and Groleau and Musy who are in the opposite situation, the authors get a mass flow rate from the left to right cavity higher than that of the vertical boundary layer at mid-height of the cavity.

4.3. Pollutant diffusion behaviour

After considering the thermal and dynamic aspects of the mean flow, let us now focus on the pollutant diffusion process. Two series of one minute interval snapshots are presented in Figs. 7 and 8, from the beginning of diffusion up to 10 minutes after diffusion stops, that is over a total time of 11 minutes. DNS results are presented in Fig. 7, and a typical RANS contribution in Fig. 8. In order to complete the discussion, the pollutant flux under the lintel entering the right cavity:

$$\dot{m}_{SF_6}^+(\tau) = \int_0^{0.7H} \rho_{\text{air}} U^+(x = 3 \text{ m}, z, \tau) c(x = 3 \text{ m}, z, \tau) dz \quad (5)$$

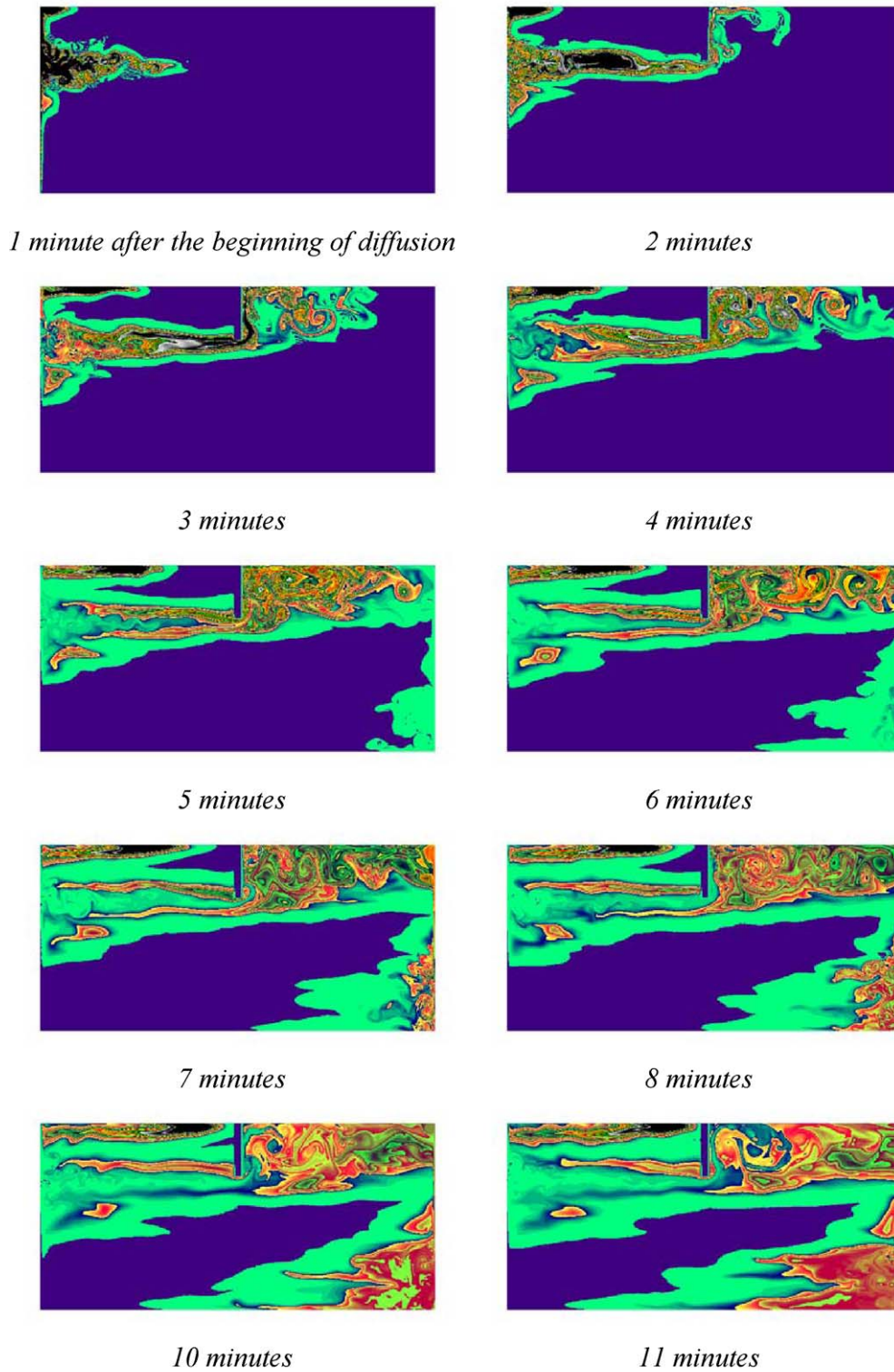


Fig. 7. DNS snapshots of the pollutant.

is presented in Fig. 9, while the mass of pollutant having entered the right cavity,

$$m_{\text{SF}_6}(t) = \int_0^t \dot{m}_{\text{SF}_6}^+(\tau) d\tau \quad (6)$$

is plotted on Fig. 10.

Note that if all the authors dealt with the pollutant diffusion process, not all of them computed the mass pollutant and flux under the lintel. This is because the required quantities for this exercise evolved with time, and for different

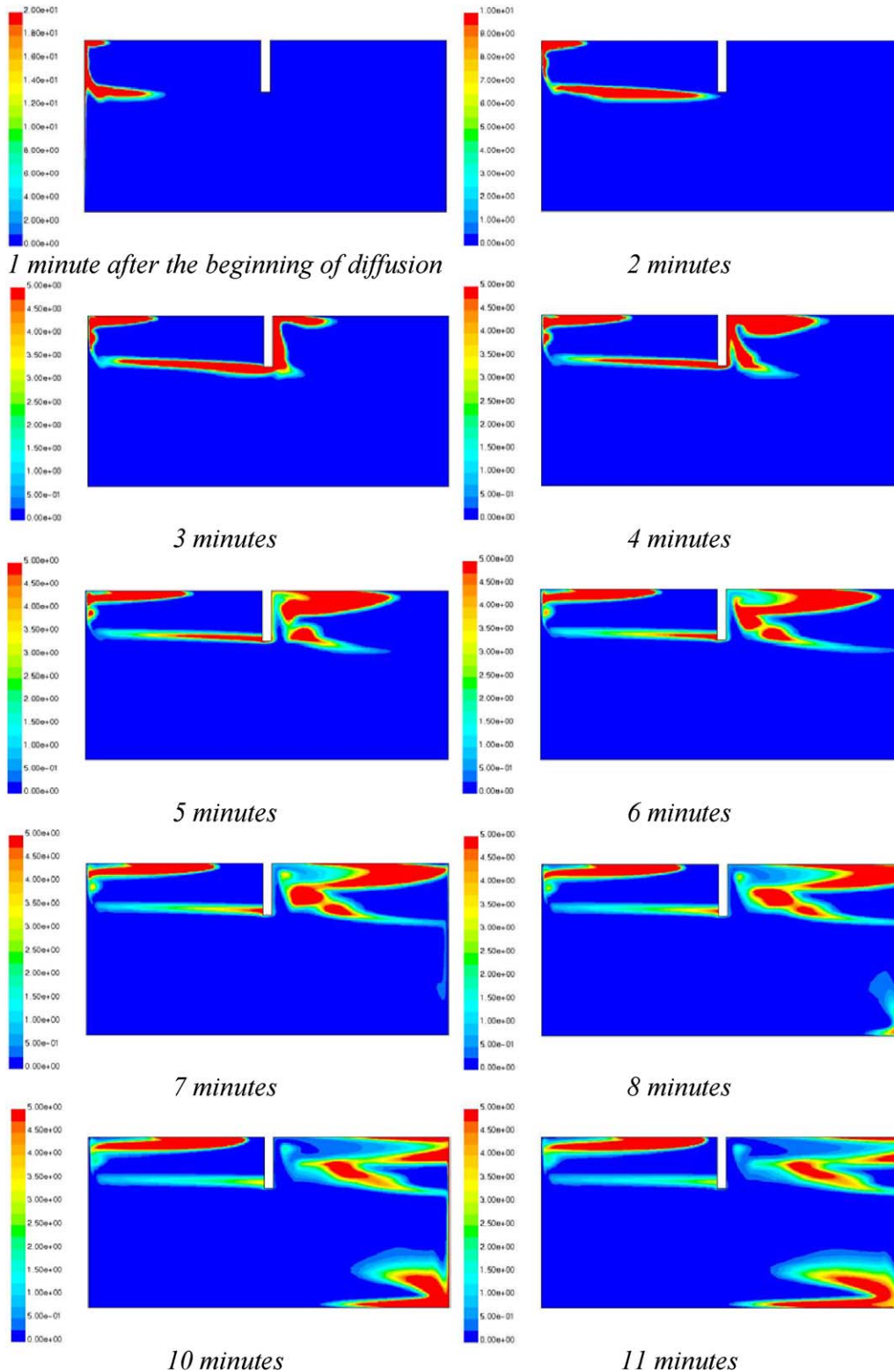


Fig. 8. An example of RANS snapshots of the pollutant.

reasons some contributors could not perform further computations. Nevertheless, at least one or more complete set of values are available for either steady RANS or unsteady DNS/LES approaches.

From a general point of view, the main difference in the behaviour of the pollutant between RANS and DNS is of course the unsteady aspects of the flow. With steady RANS approaches the pollutant is convected and diffused by the

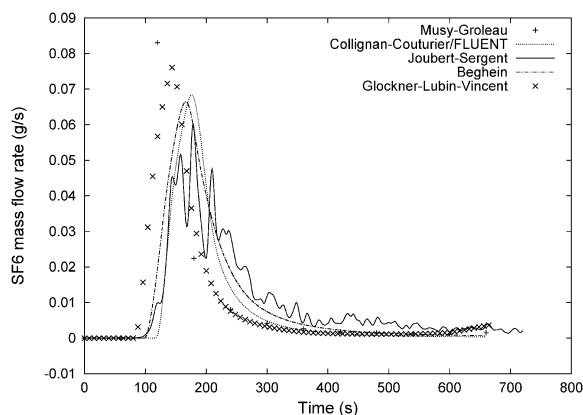


Fig. 9. Time evolution of the pollutant flux entering the right cavity.

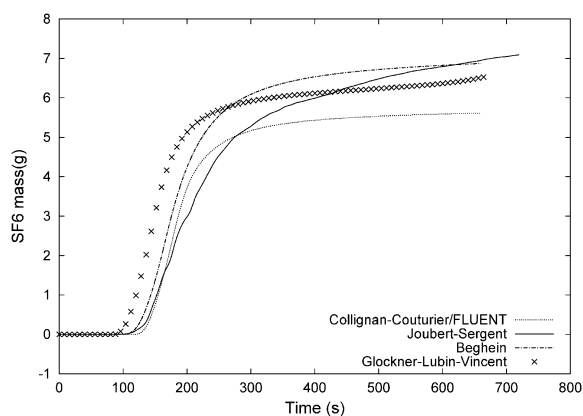


Fig. 10. Time evolution of the mass pollutant having entered the right cavity.

way of the mean flow characteristics. Therefore, the resulting behaviour is very smooth in time and space. On the other hand, the dynamic nature of DNS or LES reveals the complex instantaneous spatial structure of the flow, leading to an irregular time evolution. The pollutant then enters the right cavity intermittently, according to the interaction between the horizontal jet-like structure and the eddies detachment behind the lintel (Figs. 7 and 9).

During the one minute diffusion step, the pollutant is produced all along the left wall and dragged along by the hot vertical boundary layer. It then can be separated into two parts.

One part is convected directly to the right cavity by the horizontal jet and produces an abrupt amount of pollutant in the right cavity, with a time of maximum flux under the lintel between 120 and 175 seconds, depending on the authors.

On the other hand, another part of the pollutant is fed into the quiescent upper region of the left cavity where it remains trapped near the ceiling and then moves slowly to the lintel. Continuing time integration, we would probably observe a second smoother peak for the pollutant entering the right cavity, corresponding to this part of the pollutant going down and around the lintel. This is perhaps what is observed in the late time results of Glockner et al. because

the flux slightly grows up and produce an inflexion point for the mass of pollutant having entered the right room.

In addition to the instant of maximum flux, another value of interest is the time at which a certain quantity of pollutant has entered the second room. Depending on the value we consider, the differences can be very large. As an example, the time for which half of the total mass of pollutant came into the right cavity vary from 220 (Glockner et al.) to 380 seconds (Collignan and Couturier).

These differences can in fact have a great influence for practical problems. As an example, for accidental pollution events or chemical attacks in buildings, short time characteristics for the dispersion of pollutant are very important, because they determine the available length of time for evacuating people in safe conditions.

5. Conclusion

Some conclusions can be drawn from the comparisons between the different contributions of this comparison exercise of turbulent natural convection in partitioned cavity with pollutant diffusion:

- Large differences are observed when considering mean thermal and dynamical aspects of the flow. These differences are observed between steady RANS and DNS or LES computations, but also between the different RANS contributions, even for nearly identical spatial grid resolution.
- Nevertheless, computed Nusselt numbers at the walls lie within a $\pm 25\%$ range, that is in pretty relative good agreement regarding previous comparison exercises of the same type.

Two remarkable differences between RANS and DNS or LES mean flow fields must be highlighted:

- (1) The DNS or LES vertical boundary layers exhibit a typical laminar behaviour over a large extent of the vertical walls, approximately up to mid height, while RANS computations predict a turbulent kinetic energy production very early in the boundary layer, which result in thicker dynamical boundary layers. As a consequence, RANS approaches display a general trend to overestimate the mass flow rate through the boundary layer, compared to DNS.
- (2) Thermal stratifications predicted by DNS and LES are always larger than those corresponding to RANS. This is a persistent difference from previous comparison.

Turning now to the pollutant dispersion, the discrepancies on the dynamics lead to a large scattering for the characteristic times, either for the peak of pollutant entering the test cavity, or for the total quantity of pollutant entered this cavity.

The goal of this paper is to highlight some characteristic differences that can be observed when using various numerical softwares, even with turbulence models of the same family. As these differences can have a great influence when dealing with real life situations or engineering problems, we believe that this type of benchmark is useful to CFD users and developers and needs to be extended further.

Indeed, most of the present RANS contributions to the benchmark exercise were obtained with commercial CFD codes, using $k-\epsilon$ type turbulence modelling generally associated to a RNG formulation. Although this approach is widely used for engineering or applied research studies for complex problems, partly because of its simplicity, it is known to present severe limitations for complex flows. Particularly, the use of wall functions leads to overpredict the turbulent kinetic energy and Nusselt number, because a non-zero turbulent kinetic energy production is imposed at the first grid point when using wall functions. On the other hand, 2D DNS and LES could underestimate the level of turbulence, because the lack of vortex stretching mechanism in the third direction can result in a delay in transition as compared with full 3D simulations.

We thus believe it is of utmost interest to extend this benchmark exercise to other approaches. Additional contributions based on more sophisticated turbulence models (URANS, second order moment closures, hybrid LES/RANS . . .) are needed.

Acknowledgements

We gratefully thank the reviewers for their remarks and comments which have been of great help in improving the quality of the presentation and discussion of the results.

Supplementary material

Supplementary data associated with this article can be found, in the online version, at DOI: [10.1016/j.ijthermalsci.2004.09.005](https://doi.org/10.1016/j.ijthermalsci.2004.09.005).

References

- [1] N.C. Markatos, M.R. Malin, Mathematical modelling of buoyancy-induced smoke flow in enclosures, *Internat. J. Heat Mass Transfer* 25 (1982) 63–75.
- [2] C.P. Mao, A.C. Fernandez-Pello, J.A.C. Humphrey, An investigation of steady wall ceiling and partial enclosures fires, *J. Heat Transfer* 106 (1984) 221–228.
- [3] P.H. Thomas, Two-dimensional smoke flows from fires in compartments: Some engineering relationship, *Fire Safety J.* 18 (1992) 125–137.
- [4] Y. He, Measurement of doorway flow field in multi-enclosure building fires, *Internat. J. Heat Mass Transfer* 42 (1999) 3253–3265.
- [5] H. Manz, W. Xu, M. Seymour, Modelling smoke and fire in a hotel bedroom, in: A.K. Melikov, P.V. Nielsen (Eds.), Proceedings of the 8th International Conference on Air Distribution in Rooms, Roomvent 2002, 2002, pp. 65–69.
- [6] N. Gobeau, C.J. Saunders, Computational fluid dynamics validation of the prediction of pesticide dispersion in a naturally-ventilated building, in: A.K. Melikov, P.V. Nielsen (Eds.), Proceedings of the 8th International Conference on Air Distribution in Rooms, Roomvent 2002, 2002, pp. 81–84.
- [7] B. Collignan, S. Couturier, A.A. Akoua, Evaluation of ventilation system efficiency using CFD analysis, in: A.K. Melikov, P.V. Nielsen (Eds.), Proceedings of the 8th International Conference on Air Distribution in Rooms, Roomvent 2002, 2002, pp. 77–80.
- [8] S. Somarathne, M. Kolokotroni, M. Seymour, A single tool to access the hest and airflows within an enclosure: Preliminary tests, in: A.K. Melikov, P.V. Nielsen (Eds.), Proceedings of the 8th International Conference on Air Distribution in Rooms, Roomvent 2002, 2002, pp. 85–92.
- [9] R.A.M.W. Henkes, C.J. Hoogendoorn (Eds.), Turbulent Natural Convection in Enclosures; A Computational and Experimental Benchmark Study, Proceedings of Eurotherm Seminar 22, EETI, Paris, 1993.
- [10] R.A.W.M. Henkes, C.J. Hoogendoorn, Comparison exercise for computations of turbulent natural convection in enclosures, *Numer. Heat Transfer B* 28 (1995) 59–78.
- [11] S. Xin, P. Le Quéré, Direct numerical simulations of two-dimensional chaotic natural convection in a differentially heated cavity of aspect ratio 4, *J. Fluid Mech.* 304 (1995) 87–118.
- [12] E. Tric, G. Labrosse, M. Betrouni, A first incursion into the 3D structure of natural convection of air in a differentially heated cubic cavity, from accurate numerical solutions, *Internat. J. Heat Mass Transfer* 43 (2000) 4043–4056.
- [13] R.A.W.M. Henkes, P. Le Quéré, Three dimensional instabilities of natural convection flows in differentially heated cavities, *J. Fluid Mech.* 319 (1996) 281–303.
- [14] W. Zhang, Q. Chen, Large Eddy simulation of natural and mixed convection airflow indoors with two simple filtered dynamic subgrid scale models, *Numer. Heat Transfer A* 37 (2000) 447–463.
- [15] S.H. Peng, L. Davidson, Large Eddy simulation for turbulent flow in a confined cavity, *Internat. J. Heat Fluid Flow* 22 (2001) 323–331.
- [16] H.S. Dol, K. Hanjalic, Computational study of turbulent natural convection in a side-heated near-cubic enclosure at a high Rayleigh number, *Internat. J. Heat Mass Transfer* 44 (2001) 2323–2344.
- [17] P. Le Quéré, Onset of unsteadiness, routes to chaos and simulations of chaotic flows in cavities heated from the side: A review of present status, in: G.W. Hewitt (Ed.), Proceedings of Heat Transfer 1994, the Tenth Heat Transfer Conference, 1994, pp. 281–296.
- [18] F.X. Trias, M. Soria, C.D. Pérez-Segarra, A. Oliva, DNS of natural convection in a differentially heated cavity. Effect of the three-dimensional fluctuations, in: K. Hanjalic, Y. Nagano, M. Tummers (Eds.), Proceedings of Turbulence, Heat and Mass Transfer 4, Begell House, 2003, pp. 335–342.
- [19] J. Salat, S. Xin, P. Joubert, A. Sergent, F. Penot, P. Le Quéré, Experimental and numerical investigation of turbulent natural convection in a large air-filled cavity, *Internat. J. Heat Fluid Flow* 25 (2004) 824–832.
- [20] T. Fusegi, J.M. Hyun, K. Kuwahara, Numerical simulations of natural convection in a differentially heated cubical enclosure with a partition, *Internat. J. Heat Fluid Flow* 13 (1992) 176–183.
- [21] K. Hanjalic, S. Kenjeres, F. Durst, Natural convection in partition two-dimensional enclosures at higher Rayleigh numbers, *Internat. J. Heat Mass Transfer* 39 (1995) 1407–1427.
- [22] M.W. Nansteel, R. Greif, Natural convection in undivided and partially divided rectangular enclosures, *J. Heat Transfer* 103 (1981) 623–629.
- [23] M.W. Nansteel, R. Greif, An investigation of natural convection in enclosures with two and three dimensional partitions, *Internat. J. Heat Mass Transfer* 27 (1984) 561–571.
- [24] D.A. Olson, L.R. Glicksman, H.M. Ferm, Steady state natural convection in empty and partitioned enclosures at high Rayleigh numbers, *J. Heat Transfer* 112 (1990) 640–647.